Environmental Earth Sciences (2023) 82:536
https://doi.org/10.1007/s12665-023-11227-0

ORIGINAL ARTICLE

Coupling major ions and trace elements to turbidity dynamics for allogenic contribution assessment in a binary karst system (Sierra de Ubrique, S Spain)

Jaime Fernández-Ortega[1] · **Juan Antonio Barberá**[1] · **Bartolomé Andreo**[1]

Received: 24 July 2023 / Accepted: 7 October 2023 / Published online: 28 October 2023

Abstract
This investigation deals with the application of a multi-technique approach combining data from turbidity, major ions, and trace elements to characterize the implications of allogenic recharge in a binary karst system and assess the relative hydrochemical contribution to karst springs captured for drinking use. Hydrodynamic and hydrochemical responses of the outlets to storm events were continuously monitored during four selected flooding events, and water samples were collected at the main sinking stream in the recharge area and discharge points (Cornicabra and Algarrobal springs) for chemical analysis. The obtained hydrogeochemical dataset was analyzed through mean of time-series and statistical analysis and allowed to describe the fate and origin of trace elements. Despite that most of analyzed components present a natural origin, the existence of a Wastewater Treatment Plant in the recharge area was determined to be the main source of P (phosphorus) concentrations measured in the karst springs. Sediment (particulate) transport constitutes the most important factor in the mobilization of Al, Mn, Ni, and Ba in both surface and groundwater, whilst Li, Sr, and P are mainly controlled by solute migration. The hydrochemical signature of allogenic water component was constrained by identifying characteristic correlations between Ba and Ca/Sr ratio in water samples. The combination of specific hydrogeological processes as ion solution and sorption processes onto solids between solutes and particles as well as water mixing processes (allogenic vs diffuse) result more evident in Algarrobal spring, which receives a higher contribution of allogenic component due to a greater feeding catchment.

Keywords Karst aquifer · Turbidity · Trace elements · Groundwater/surface–water relationships · Southern Spain · Binary karst · Drinking water

Introduction

Karst aquifers constitute a reliable drinking water source worldwide (Stevanović 2019) and a strategic resource in mountainous regions. However, karst aquifers are highly vulnerable to contamination due to the absence of thick filtering soils and the presence of preferential flowpaths that favour fast groundwater movement due to circulation through a—very often—well-developed conduit network (Goldscheider and Drew 2007). Highly karstified carbonate aquifers are well known for the rapid response to intense rain events which result in quick variations of hydrochemical parameters and, in some cases, high turbidity peaks and elevated concentrations of suspended particles and colloids in karst springs (Pronk et al. 2007; Goldscheider 2005). The arrival of suspended sediments (which originate turbidity) and associated contamination (e.g., trace elements) also presents sanitary implications and shows health risks caused by disease transmission or heavy metal accumulation in human bodies (U.S. EPA 2018).

Studies about the presence of mobile sediments in karst aquifers have been developed throughout the last decades; and among these, three classes are traditionally differentiated (Grolimund et al. 2007): (i) colloidal particles, precipitates of inorganic pollutants; (ii) carrier colloidal particles, which bind the pollutants at their surfaces) and, (iii) biocolloids, such as bacteria or viruses. Fine grain sediments in karst systems (topics i and ii) may present two different sources: autochthonous, sediments derived from carbonate

✉ Jaime Fernández-Ortega
jaimeortega@uma.es

[1] Department of Geology and Center of Hydrogeology (CEHIUMA), Faculty of Sciences, University of Málaga, 29071 Málaga, Spain

matrix dissolution, and allochthonous, sediments washed by runoff waters and introduced through swallow holes or sinking streams into the system during flooding events (Mahler et al. 1999; Feeser and O'Connell 2009; Yang et al. 2010). In binary karst systems, allogenic recharge has been demonstrated to have direct implications in groundwater quality due to the transport capability of large amounts of sediments (Ryan and Meiman 1996; McCarthy and Shevenell 1998; Mahler and Lynch 1999; Shevenell and McCarthy 2002). Transport mechanisms of sediments in karst aquifers might depend on hydrogeological factors, such as length or drainage network geometry, chemical species, or type of source (Ryan and Meiman 1996; Currens 1997; McCarthy and Shevenell 1998).

In karst groundwater, the existence of suspended or diluted particles, colloids, or chemically bounded to cationic species has been traditionally used to explain enhanced transport of trace elements (McCarthy and Shevenell 1998; Mavrocordatos et al. 2000). Sorption processes because of electrostatic forces between trace elements and colloidal and suspended sediments have been widely described and such mechanisms might then act as an important transport vector in surface and groundwater (Hart 1982; Jenne and Zachara 1987; Horowitz 1991; Zimmerman 1993). During flooding events, the transport of chemical species sorbed onto solids is more complex due to the increase in suspended sediments and changes in their composition (Atteia and Kozel 1997; Mahler and Lynch 1999; Mahler et al. 1999).

Major and trace elements are naturally released from minerals due to the host-rock weathering and then retained in soils or drained into water bodies. Natural colloidal particles can be composed of inorganic material originating from the rock, such as clays minerals, zeolites, quartz, feldspars, Fe-oxides, and hydroxides (McCarthy and McKay 2004). Thus, in natural conditions, the background concentration in soils of such elements directly depends on the mineralogical composition of rocks and weathering processes to which a specific area has been exposed to (Adriano 1986). Mechanisms controlling the mobilization of such elements, their transformation, and redistribution depend on physical, geochemical, and biological processes such as topography and/or runoff generation, mineral dissolution rates, or biomineralization (De Kimpe et al. 1984; Elderfield et al. 1996; Sandén et al. 1997; Stallard 2012; Buss et al. 2017). Chemical variables of the soils such as redox conditions might also favour dissolution or precipitation processes resulting in characteristic trace-element signals in soils (Durn et al. 2021). However, common human activities, such as mining, steel industry, cement plants, and domestic wastewaters (Li et al. 2013; Dragović et al. 2014; Kong 2014; Cutillas-Barreiro et al. 2016; Turner 2019), very often result in soil contamination by trace elements and may present direct implications in groundwater protection. In natural karst systems, a little number of studies dealing with trace elements analysis have been carried out probably due to the low background concentrations measured in absence of geochemical anomalies in the host-rock mineralogy (e.g., ore deposits) or anthropogenic activities (e.g., urban wastes, mining or chemical industries, etc.). Nowadays, the study of aqueous trace-element geochemistry linked to suspended sediment dynamics has emerged as a powerful tool for fingerprinting groundwater origin in karst aquifers (Gill et al. 2018).

In the present research, the simultaneous response of two permanent karst springs used for water supply in a binary carbonate aquifer to four consecutive precipitation events was analyzed. The rainfall accumulation and intensity during these events were high enough to generate a hydrodynamic and hydrochemical response at such outlets. The overall goal of this research is to estimate the aquifer's vulnerability to the contamination which could help to improve the management of groundwater sources used for drinking water supply. Hence, this work primarily aimed to assess the fate and origin of selected trace elements and to define transport mechanisms that control their mobilization, emphasizing on the implications of suspended sediments dynamics. Furthermore, this study further estimates the relative influence of allogenic recharge in terms of chemical variability at the karst springs and sediment input into the system which cause periods of poor quality for human consumption.

Site description

Ubrique test site

In the study site, Sierra de Ubrique carbonate massif is found within the limits of Sierra de Grazalema Natural Park and reaches altitudes ranging from 400 to 1500 m above sea level (asl). This mountainous area is located in the eastern part of the Cádiz province (approximately 80 km NE from Cádiz city, S Spain) (Fig. 1A, B). The climate in this area is semi-continental Mediterranean and rainfall mainly occurs in autumn and winter, associated with wet winds coming from the SW. Mean annual rainfall is 1305 mm (period 1984/85–2017/08) (Martín-Rodríguez et al. 2023). Land use is mainly linked to a population of 500 inhabitants and its related activities are the extensive livestock and the cheese industry with several alimentary factories. Urban waters are treated in a little wastewater treatment plant (storm water tanks).

Soil development within the study area is generally scarce and, in some areas, practically non-existent due to the steep orography and the presence of carbonate outcrops. Its distribution is limited to topographically depressed areas, such as sinkholes and uvalas, filled by *Terra rossa* clays or to outcrops of low permeability materials located in the perimeter

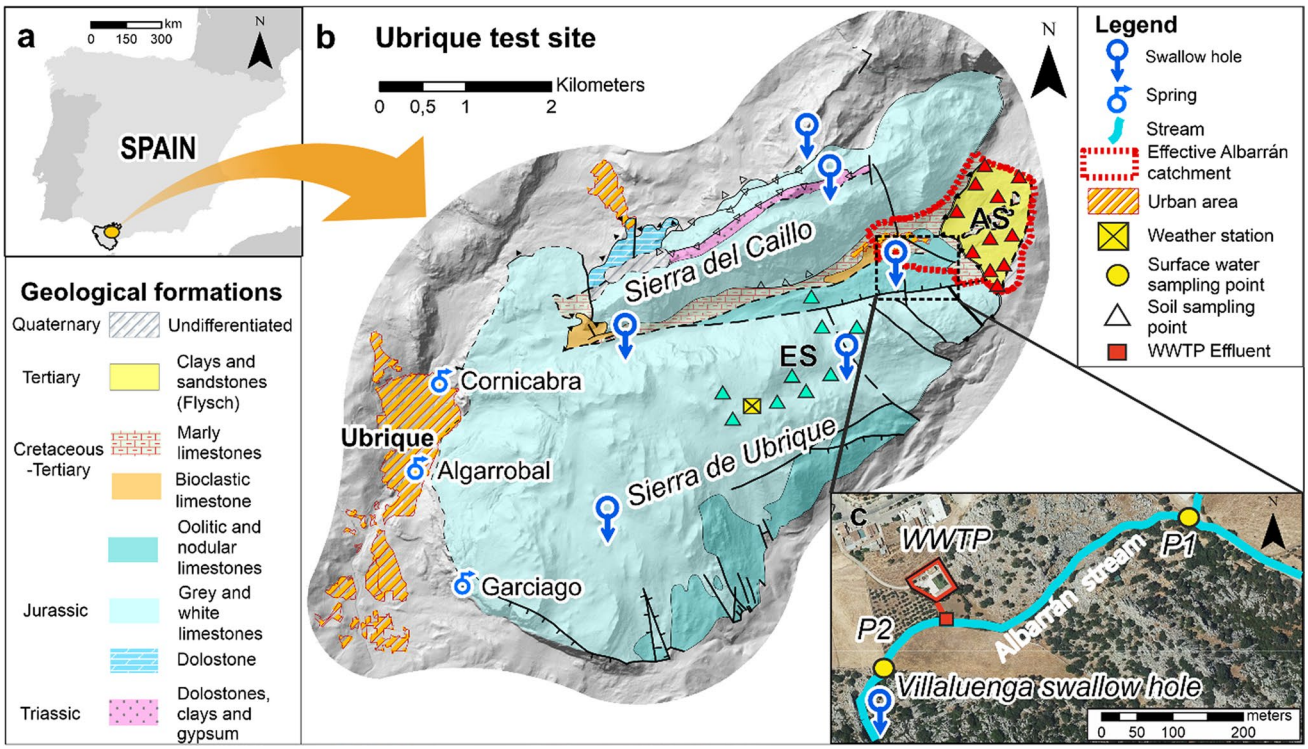

Fig. 1 Location map at country scale (**A**). Geological and hydrogeological setting of the study site (**B**). Zoomed out area of the allogenic infiltration site in the Sierra de Ubrique aquifer (**C**)

zones of the study area. As a general trend, two main types of soil are distinguished: the carbonate outcrops are covered by patchy leptosols and cambisols, whereas less permeable soils with a thickness of 10–70 cm and a silty–clayey texture overlie Cretaceous marl outcrops.

From a geological standpoint, Sierra de Ubrique is located within the External Zones of the Betic Cordillera (formed during the alpine orogeny). The geological formations that mainly define the area are (from bottom to top, Fig. 1B): Upper Triassic (Keuper) clays, sandstones and evaporite rocks (mainly gypsum), Jurassic dolostones (lower) and limestones (upper)—500 m thick, and Cretaceous-Paleogene marly-limestones and marls (Martín-Algarra 1987). In addition, overthrusting all the Mesozoic rock sequence, Tertiary clay and sandstone flysch type formations (Campo de Gibraltar unit) are found. The geological structure is characterized by fractured box-shaped anticline folds which axes dive towards the NE and synclines matching with depressions constituted by younger marly-limestones materials as well as recent strike-slip faults (NW–SE) and normal fractures (NNW–SSW and N–S) (Martín-Algarra 1987).

During intense rain episodes, usually > 10 mm/h, runoff is produced over the flysch clays that compose the Albarrán stream (3 km^2) catchment (Fig. 1B) generating a variable flow (ranging from 1 to 4000 L/s) with elevated turbidity (up to 260 NTU) that sinks through the Villaluenga swallow hole (Fig. 1C). In addition, the discharge point of the Waste Water Treatment Plant (WWTP) of Villaluenga village (500 inhabitants) is located 200 m upstream from Villaluenga shaft. Other minor endorheic areas developed in clayey—*Terra rossa*—materials may also produce runoff flow in the higher areas of Sierra del Caillo and Sierra de Ubrique (Fig. 1B).

Recharge mainly occurs by diffuse infiltration from rainfall through carbonate outcrops (approximately 26 km^2) and by allogenic contribution from the previously described Albarrán stream catchment. The hydrogeological functioning of this fractured and karstified aquifer is thus characterized by duality in recharge mechanisms, proved through dye tracer techniques (Martín-Rodríguez et al. 2023). The two main natural discharge points draining Sierra de Ubrique aquifer are located in the SW border: Cornicabra (349 m a.s.l., average discharge 270 L/s) and Algarrobal (317 m a.s.l., average 372 L/s) (Martín-Rodríguez et al. 2023). Additionally, the overflow spring Garciago (422 m asl) appears in the SW edge during flooding events and ranges from 0 to 5042 L/s (Sánchez et al. 2018).

The main hydrogeological karst connections were proved by the performance of two tracer tests (Martín-Rodríguez et al. 2023) that provided valuable information about travel times (31 h in Cornicabra, 47 h in Algarrobal and 45 h in Garciago) and the estimation of the allogenic recharge contribution through Villaluenga swallow hole (≈ 6 km far from

the springs). Maximum velocity reached by the tracer to each of those sampling points was 177.6, 129.9, and 144.3 m/h, respectively. Recovery rates of the tracer injected at that point resulted in 2% in Cornicabra, 21.9% in Algarrobal, and 68.4% in Garciago springs. However, only Cornicabra and Algarrobal are permanent springs and only they are both used for water supply Ubrique town. This experiment revealed the karst connections between the recharge area and the main springs draining Sierra de Ubrique aquifer under certain hydrodynamic conditions.

Materials and methods

Groundwater and soil sampling

A total of five water points (surface and groundwater) were sampled in this study. Three of them are located in the recharge area, including the discharge point of the WWTP effluent and two surface water points at the Albarrán stream (upstream of the effluent, P1 and downstream, P2, Fig. 1C). The remaining monitored points are the two permanent springs (Cornicabra and Algarrobal springs; Fig. 1B) that drain the karst system. The sampling procedure included (1) monthly samples of the WWTP effluent, (2) daily runoff samples during the activation of Albarrán stream and (3) daily manually taken-groundwater samples at the springs. Furthermore, sampling rate at permanent springs was increased to 4 h through the use of an autosampler (Teledyne ISCO 3700®) during flooding events.

Water samples were taken in conic-shaped plastic vials and acidified with a 1:10 dilution of high analytical grade HNO_3 (C.A.S.: 7697-37-2) in Milli-Q® ultra-pure water for trace-element analysis and 125 ml brown glasses for chemical analysis of major ions. Both kind of samples are filtered with a 0.45 µm cellulose acetate (CA) filter. Water samples were stored in the dark and refrigerated until its analysis in the laboratory no later than 2–3 days.

A total of 20 soil samples were taken between 5 and 10 cm depth at two sampling areas: the (clayey—*Terra rossa*) epikarst soil ($n = 9$, referred as ES hereafter, Fig. 1C) in Sierra de Ubrique and the (clayey–flysch) Albarrán stream catchment soil ($n = 11$, AS, Fig. 1C) using nitrile gloves and a hard-plastic shovel and bags to avoid the contamination of the samples. Soil samples were stored in the dark and refrigerated until its digestion in the laboratory no later than 2–3 days.

The methodological approach is shown in Fig. 2, including both field and laboratory techniques.

Field devices

Physico-chemical parameters such as Electrical Conductivity (EC) and temperature were in-situ measured in the selected water points with a conductivimeter/thermometer WTW™ Cond 3110 in addition to pH and Oxidation–Reduction Potential—ORP—using a HACH™ multiprobe HQ40D. Turbidity was measured using a pocket turbidimeter HACH™ 2100Qis. Two different devices for obtaining continuous records of water parameters were set in the permanent springs with a 15 min measuring rate. Those parameters are water level (Odyssey® from Dataflow Systems Ltd, NZ), as well as temperature, electrical conductivity, and turbidity (GGUN FL30® from Albilia SARL, SZ). Accumulated rainfall was determined hourly at Sierra de Ubrique (Fig. 1B) using a weather station Davis Vantage Pro™ installed at an altitude of 1029 m a.s.l.

Laboratory analysis

Samples were processed in the laboratory of the Centre of Hydrogeology of the University of Malaga (CEHIUMA).

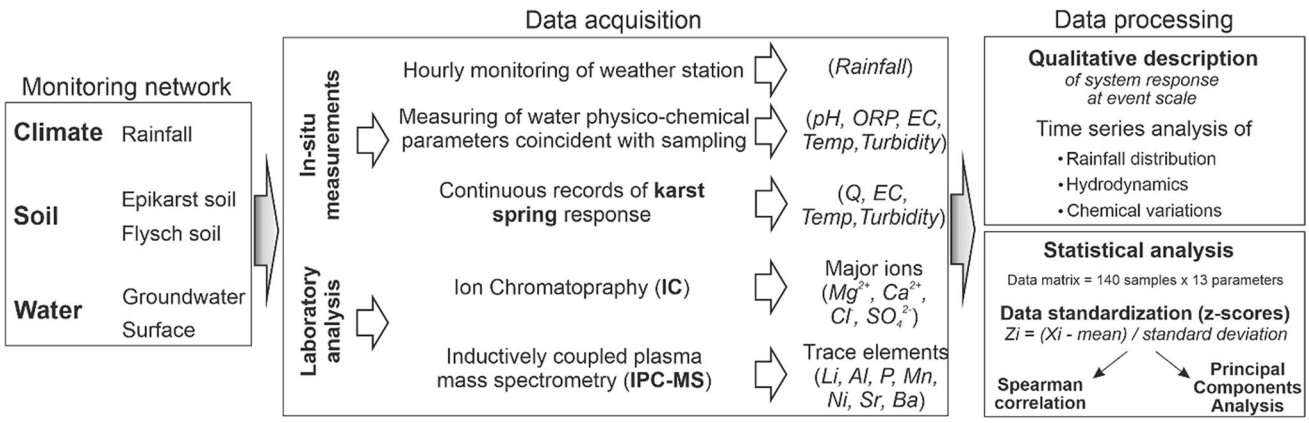

Fig. 2 Methodological flowchart applied in the framework of this research

Analyses of major ions (Mg^{2+}, Ca^{2+}, Cl^{-}, and SO_4^{2-}) were realized with an ionic chromatograph Metrohm® mods. 881 Compact IC pro and 930 Compact IC Flex and HCO_3^{-} with an automatic titrator Metrohm® mod. 888 Titrando with 2% accuracy. The quality of major ions data was assessed using the Charge Balance Error (CBE). The mean CBE value for the whole sample set was 0.5% and groundwater samples with CBE higher than ± 5% were not considered.

The digestion of soil samples was realized following the U.S. EPA (1996) standards. Water samples were previously filtered with 45 µm CA mesh. Trace elements were analyzed in groundwater and digested soil samples through the use of an Inductively Coupled Plasma Mass Spectrometry (ICP-MS) (Thermo™ Scientific ICAP-RQ, USA). From a total of 35 trace elements, 7 of them (Li, Al, P, Mn, Ni, Sr, and Ba), which present values higher than their respective detection limits, have been selected.

Trace-element data quality was assessed through the calculation of the Limit of Detection (LoD) and Limit of Quantification (LoQ) on each analysis series. Mean values of these parameters were obtained in eight analysis series and vary for each element as follows: Li (LoD = 0.02 µg/L; LoQ = 0.06 µg/L), Al (1.05; 3.52), P (1.21; 15.02), Mn (0.29; 0.99), Ni (0.18; 0.59), Sr (0.07; 0.24), and Ba (0.28; 0.95). Measurements below LoD were not considered for this research.

Results

Trace elements in soil samples

The main statistical data descriptors (maximum, minimum, mean, and standard deviation) of selected trace-element concentrations in both Sierra de Ubrique (ES) and Albarrán stream catchment (AS) soil sampling areas are presented in Table 1 and displayed in Fig. 3.

In this study, Al shows the higher mean concentration in both soils (43,180 ppm in ES and 42,935 ppm in AS) among the measured trace elements and, like Mn, presents mean values of the same magnitude in both sampling areas (Table 1). Higher mean concentrations of elements, such as Li and Ni, were found in ES compared to AS. This fact is especially noticeable in the case of P, which presents mean concentrations in soil of 4069 ppm (ES) and 745 ppm (AS). The opposite situation is observed for Sr and Ba, which were found in higher mean concentrations in AS (186 and 456 ppm, respectively) rather than ES (34 and 191 ppm, Table 1).

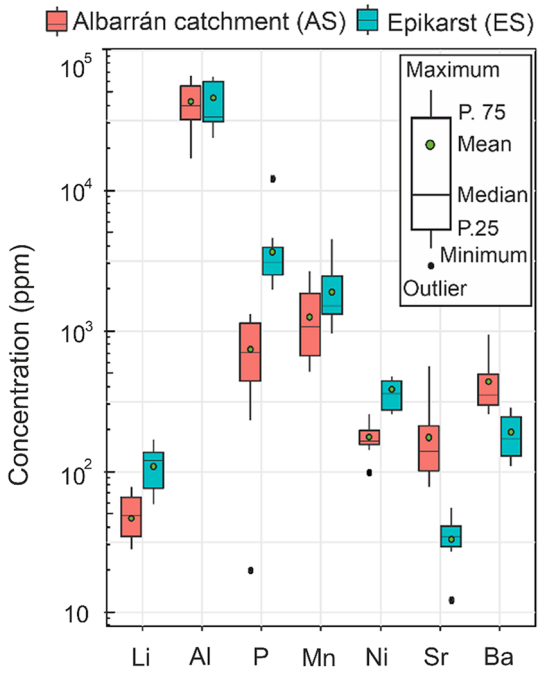

Fig. 3 Box plots of trace-element concentration in Epikarst soil—ES—(blue) and Albarrán catchment soil—AS—(red)

Physico-chemical parameters, and major ions and trace elements in water samples

Table 2 summarizes the main statistical data of physico-chemical parameter datasets (electrical conductivity, temperature, turbidity, pH, and Oxidation–Reduction Potential)

Table 1 Statistical descriptors (maximum, minimum, mean, and standard deviation) of trace elements in epikarst soil from Sierra de Ubrique (ES) and Albarrán stream catchment (AS) soil samples

Sampling point	Statistical parameter	Li (ppm)	Al	P	Mn	Ni	Sr	Ba
ES ($n = 9$)	Max	167	63,819	12,290	4452	478	55	287
	Min	58	23,772	1972	951	256	12	109
	Mean	110	43,180	4069	1980	360	34	191
	SD	37	16,476	3199	1113	85	12	72
AS ($n = 11$)	Max	77	66,083	1316	2641	252	560	936
	Min	27	16,820	20	514	98	78	256
	Mean	50	42,935	745	1316	176	186	456
	SD	18	15,522	443	801	44	138	244

Table 2 Statistical data descriptors of physico-chemical parameters measured in runoff waters, WWTP effluent, and karst groundwater samples

		Runoff P1	WWTP effluent	Runoff P2	Cornicabra	Cornicabra (taken with autosampler)	Algarrobal	Algarrobal (taken with autosampler)
	n	8	13	12	53	100	54	132
Electrical conductivity (µS/cm)	Max	353	1891	317	487	280	515	403
	Min	156	410	126	227	241	256	246
	Mean	232	1015	234	277	262	320	328
	SD	65	416	67	32	11	38	30
Temperature (°C)	Max	12.5	18.1	13.9	14.6	14.5	16.4	15.2
	Min	9.0	9.8	7.2	14.2	11.2	14.1	9.2
	Mean	11.1	13.8	11.0	14.4	13.2	15.0	13.5
	SD	1.3	2.8	1.9	0.1	1.1	0.4	1.6
Turbidity (NTU)	Max	259	999	247	53	48	270	387
	Min	2	15	6	0.5	0.5	0.3	0.5
	Mean	80	278	76	4	6	19	60
	SD	92	342	85	7	5	46	77
pH	Max	8.7	8.6	8.9	8.2	8.4	8.2	8.5
	Min	7.3	7.1	8.3	7.0	7.9	7.0	7.5
	Mean	8.1	7.7	8.6	7.8	8.2	7.8	8.1
	SD	0.4	0.4	0.2	0.3	0.1	0.2	0.2
Oxidation–reduction potential (mv)	Max	247.8	242.6	472.9	383.7	704.8	403.8	540.7
	Min	15.7	−298.1	124.6	46.6	165.0	75.2	101.2
	Mean	104.4	−47.3	242.9	184.9	366.0	206.1	229.5
	SD	93.9	194.4	96.8	65.9	152.5	65.2	71.9

measured in both surface and groundwater samples. Runoff waters show a low mineralization (mean EC values) compared to Cornicabra and Algarrobal springs samples. However, maximum turbidity values in runoff (P1 and P2) are of the same magnitude than those measured in Algarrobal spring (rather than Cornicabra spring, Table 2). The pH values in the springs vary between 7 and 8.2 in hand samples and show mean values slightly lower than those measured in runoff samples. A greater oxidation potential (higher ORP values) is observed in P2 point and Algarrobal spring waters in comparison to P1 point and Cornicabra spring, respectively. The data obtained from the WWTP Effluent are distributed in a wider range regarding maximum values of EC, Turbidity, and ORP.

Statistical parameters of chemical analysis from most of ions (Table 3) present as well quite high mean values of Cl^- and P in the WWTP effluent samples. Unlike that happens with other ions, the mean concentration of such parameters is significantly higher in P2 compared to P1. Maximum P concentration measured in P1 (359 µg/L) is much lower than in P2 (2052 µg/L), which value is of the same order of magnitude as mean P concentration in WWTP Effluent (2629 µg/L).

Runoff (P1 and P2) samples present higher mean content of SO_4^{2-} and Cl^- (between 9.6 and 15.6 and 4.5 and 9 mg/L, respectively) and lower of HCO_3^- (133.5–152.6 mg/L) and Ca^{2+} (38.5–49.3 mg/L) compared to karst spring samples (Table 3). Generally, data from P1 and P2 depict higher mean concentrations of trace elements compared to groundwater, except Al, Mn, and Ni, which present slightly higher mean values in Algarrobal spring (Fig. 4).

Regarding groundwater samples, higher mean and maximum values of major ions (specially SO_4^{2-} and Cl^-, Table 3) and the EC and turbidity ones (Table 2) are observed on Algarrobal spring. Trace-element data show a greater dispersion in the samples from P2 (Fig. 4). Algarrobal spring also shows higher mean concentration values of all trace elements compared to Cornicabra, among which, Al (147.8 vs 37 µg/L), P (102 vs 17.8 µg/L), and Mn (57.6 vs 8.4 µg/L) are specially remarkable in the most representative record of samples collected with autosampler (Table 3).

Table 3 Summary of the main statistics (maximum, minimum, mean, standard deviation, and median) of selected trace elements and major ions in runoff water, WWTP effluent, and karst groundwater samples

Sampling point	Statistical parameter	HCO_3^- (mg/L)	Ca^{2+} (mg/L)	Mg^{2+} (mg/L)	Cl^- (mg/L)	SO_4^{2-} (mg/L)	Li (µg/L)	Al (µg/L)	P (µg/L)	Mn (µg/L)	Ni (µg/L)	Sr (µg/L)	Ba (µg/L)
Runoff P1	*n*	8	8	8	8	8	8	8	7	7	8	8	8
	Max	245.2	83.5	10.0	14.8	64.2	10.8	381.6	359.4	131.1	3.4	108.9	538.1
	Min	95.8	29.4	1.6	0.9	3.9	1.3	19.9	22.5	1.5	0.7	32.6	71.9
	Mean	152.6	49.3	4.0	4.5	15.6	3.6	139.5	139.5	49.2	1.9	54.6	204.3
	SD	53.5	19.8	2.6	4.7	20.1	3.1	115.3	151.9	55.9	1.0	27.8	182.6
	Median	147.2	45.4	3.3	2.9	9.2	2.4	101.8	45.2	16.2	1.6	42.6	127.7
WWTP effluent	*n*	13	13	13	13	13	13	12	13	12	13	13	13
	Max	523.5	135.2	20.2	419.0	32.6	7.4	110.9	6761.9	91.8	6.0	138.9	460.1
	Min	173.0	54.8	3.8	9.7	0.4	2.2	9.5	360.2	12.7	0.6	40.8	47.0
	Mean	364.9	83.6	11.1	154.3	14.7	5.3	64.0	2629.6	53.5	3.1	84.1	120.0
	SD	106.4	22.3	5.3	125.6	9.3	1.5	34.6	1675.2	26.8	1.7	24.0	106.5
	Median	369.9	82.3	10.3	150.2	12.2	5.4	65.6	2551.6	60.0	3.2	87.0	95.1
Runoff P2	*n*	12	12	12	12	12	12	11	9	12	12	12	12
	Max	207.5	60.7	5.2	29.8	19.5	8.9	264.6	2052.7	99.0	3.2	194.0	710.7
	Min	53.9	13.2	0.2	0.2	2.0	0.6	58.7	11.4	0.5	0.4	8.4	7.9
	Mean	133.5	38.5	3.0	9.0	9.8	3.3	121.2	529.8	24.8	1.5	53.0	225.7
	SD	47.8	14.7	1.6	10.0	5.7	2.3	68.1	631.7	26.8	0.7	47.9	232.1
	Median	133.6	38.0	3.3	3.2	10.3	3.1	93.5	413.2	16.2	1.5	41.7	87.7
Cornicabra	*n*	53	53	53	53	53	53	47	26	48	50	53	53
	Max	193.8	67.9	3.3	4.7	8.2	2.8	228.7	257.4	48.2	5.7	343.3	65.6
	Min	155.7	48.5	0.4	1.2	0.1	0.1	1.1	0.6	0.4	0.2	34.5	6.5
	Mean	179.3	59.2	1.5	2.9	3.6	0.5	28.7	30.4	5.4	2.5	76.4	16.6
	SD	8.9	4.2	0.6	1.1	2.7	0.4	44.8	63.6	9.9	1.3	53.4	10.0
	Median	181.8	58.3	1.4	3.2	2.9	0.4	11.7	9.1	1.8	2.1	62.8	14.2
Cornicabra (taken with autosampler)	*n*	100	100	100	100	100	100	100	47	98	93	100	100
	Max	193.5	59.7	2.3	6.5	6.2	1.5	133.0	54.7	31.7	1.6	26.4	16.0
	Min	158.6	42.8	0.6	1.3	0.7	0.0	2.4	1.4	0.4	0.2	9.7	9.0
	Mean	176.3	54.5	1.1	2.5	1.7	0.5	37.0	17.8	8.4	0.6	14.4	12.2
	SD	9.4	4.1	0.4	0.8	1.2	0.2	24.3	13.2	7.0	0.3	3.2	1.6
	Median	178.2	55.7	1.1	2.4	1.2	0.5	28.5	15.7	6.0	0.6	13.7	11.9

Table 3 (continued)

Sampling point	Statistical parameter	HCO_3^- (mg/L)	Ca^{2+} (mg/L)	Mg^{2+} (mg/L)	Cl^- (mg/L)	SO_4^{2-} (mg/L)	Li (µg/L)	Al (µg/L)	P (µg/L)	Mn (µg/L)	Ni (µg/L)	Sr (µg/L)	Ba (µg/L)
Algarrobal	*n*	54	54	54	54	54	54	44	23	37	54	51	53
	Max	251.2	84.0	4.9	17.1	16.1	4.0	486.9	357.6	185.2	9.7	163.6	83.1
	Min	162.5	51.9	0.9	2.2	1.1	0.3	2.0	0.1	0.3	0.8	45.2	11.2
	Mean	190.4	61.5	3.3	8.5	8.2	0.9	61.3	35.0	27.6	2.9	83.9	28.3
	SD	25.8	8.3	1.2	3.5	4.4	0.6	104.1	80.5	47.2	1.6	27.0	12.0
	Median	178.6	60.1	3.8	8.0	8.0	0.7	13.5	7.3	3.8	2.4	75.7	26.5
Algarrobal (taken with autosampler)	*n*	132	132	132	132	132	131	125	61	119	107	131	117
	Max	263.9	84.3	4.3	17.1	15.3	3.5	605.8	756.1	218.5	6.5	47.9	59.8
	Min	158.5	45.6	1.0	2.4	1.2	0.1	10.4	2.7	1.0	0.4	14.6	12.6
	Mean	215.0	67.8	1.9	6.4	4.8	1.1	147.8	102.0	57.6	1.8	24.6	25.6
	SD	22.0	8.5	0.6	2.7	3.0	0.6	131.3	158.3	47.8	1.2	6.5	6.9
	Median	216.4	68.8	1.9	5.9	4.0	1.0	122.6	24.6	44.0	1.5	23.2	25.0

Spring response during specific flooding events

Cornicabra spring

Four rain episodes (Fig. 5) of a variable accumulated precipitation (ranging from 72 to 288 mm) provoked the activation of Villaluenga shaft as well as the individual flooding events in the studied karst springs with distinctive hydrogeological responses. Cornicabra spring tipically showed a maximum discharge between 800 and 1500 L/s and a fast discharge increase during the first 12–24 h of a precipitation event. Electrical conductivity record normally shows fast decreases followed by low mineralization intervals (≈270 µS/cm) during the periods of highest spring discharge (> 300 L/s) (Fig. 5). As a general trend, turbidity record depicts one or two major peaks and multiple relative maximums coinciding with the beginning of the rising limb of the spring hydrograph. An exceptional maximum (64 NTU) in the first effective recharge event of the hydrological year 2020/21 is observed (Event 1; Fig. 5). However, the successive turbidity peaks do not exceed 15 NTU despite that a higher accumulated precipitation occurred in the last two events (Events 3 and 4, Fig. 5).

Despite such usual variations of physico-chemical parameters, the response of major ions and trace elements presents specific singularities on each flooding event. Event 1 (Fig. 5) displays the most clear and abrupt chemical variations, with peaks of HCO_3^- and Ca^{2+} (that slightly anticipate the turbidity peak) followed by a decrease of all major ions. Event 2 shows a soft response to the precipitation episode, since no clear dilution is observed in the EC record, although there is an increase in temperature after the turbidity peak. In this event, the only notable variation of major elements is a decrease of SO_4^{2-} and Cl^- after the peak of turbidity, Al, Mn, and Ni (Fig. 5). Compared to the previously described flooding events, the two last (Events 3 and 4) show composite precipitation episodes (formed by more than one rain pulse) and also two turbidity relative maximums. In both events, it highlights that turbidity peaks match with a decrease of EC and major ions concentration. Other selected trace elements (Li, Ni, Sr, and Ba) do not show defined curves, but some small peaks coinciding with a turbidity maximum followed by a decrease in their concentration are observed towards the end of the event (Events 2 and 3, Fig. 5). The record of P presents different response at each rain event with not defined pattern. As a general trend, this spring shows poorly defined hydrochemical variations of major ions and trace elements Li, Ba, and Sr (except in the first event), but clear turbidity peaks coinciding with important EC decreases.

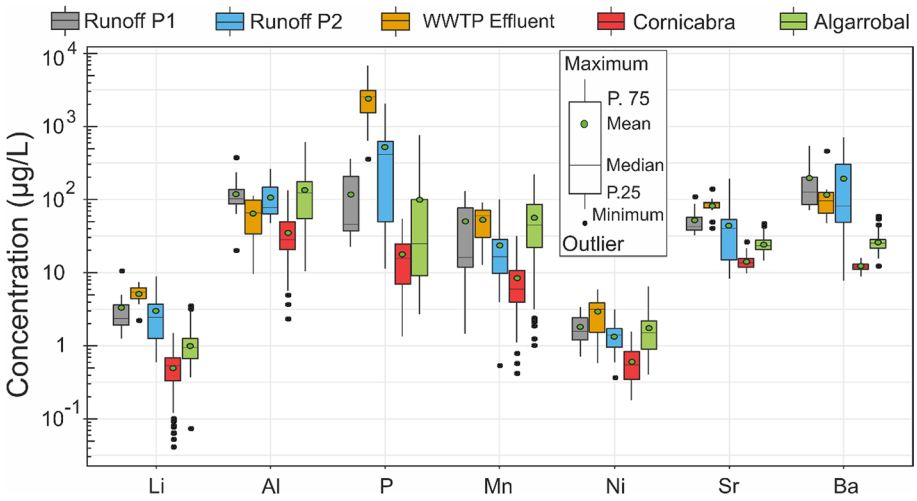

Fig. 4 Box-plot of trace-element concentration in groundwater (Cornicabra and Algarrobal springs, taken with autosampler), WWTP effluent, and surface water samples (P1 and P2, in Albarrán stream)

Algarrobal spring

The hydrodynamic behavior of Algarrobal spring shows fast increases of spring discharge and an apparent maximum threshold close to 800 L/s (Fig. 6). The variations of EC and temperature are characterized by an increase in both parameters in the first days of the event (up to ≈400 µS/cm and 15.6 °C), followed later by a significant decrease (to ≈320 µS/cm and 14.6 °C) or a return to the values prior to the flood (≈360 µS/cm and 15.2 °C) (Fig. 6). Turbidity record in Algarrobal spring shows the maximum peak (334 NTU) in the first effective rain episode of the hydrological year and relative maximum between 80 and 150 NTU in the successive flooding events (Fig. 6).

Small differences are distinguished between events: Event 1 (Fig. 6) shows the most extreme turbidity response along with the HCO_3^- and Ca^{2+} peaks and a relative peak of Cl^- (along a decreasing trend), while the other major ions (Mg^{2+}, SO_4^{2-}) show a clear decrease. Beside such major ions, trace elements show as well concentration peaks coinciding with the first turbidity peak and keep a relative high concentration along with turbidity record. The measurements of P specially highlight in this event, as it shows the maximum value of all the study period coinciding with the turbidity peak. In Event 2, although it is the least intense rain episode, it shows a turbidity maximum of 50 NTU which, in this case, coincides with high HCO_3^-, Ca^{2+}, and SO_4^{2-}. Regarding trace-element variations, Al and Mn depict variations of two orders of magnitude generally proportional to the turbidity record, while Li, Ni, Sr, and Ba show small peaks coinciding with the maximum turbidity instant. Events 3 and 4 (Fig. 6) show turbidity records with two peaks, in which the same correlation is observed between the first turbidity peak and the peaks of major ions, as well as the successive turbidity peaks and the decrease in concentration of major ions. In these events, the increase of SO_4^{2-}, Cl^- and Mg^{2+} stands out among the maximum turbidity period, as well as Li and Ba. Unlike at Cornicabra, Algarrobal spring shows greater variations of Ba with turbidity and also reproduces, to a large extent, the shape of the turbidity record. In addition, Al and Mn reproduce (again) the shape of the turbidity record and P also shows elevated peaks (200–400 µg/L) associated with turbidity peaks.

Statistical relationships between trace elements and transport vector

The different trace-element concentrations found in surface water compared to karst springs (Fig. 4) and the different behavior observed in the outlets (Figs. 5, 6) suggest that, despite the influence of suspended sediment (turbidity), other transport mechanisms and hydrochemical processes may occur. Hence, to set the relevance of transport processes within the system from a global perspective and better constrain the potential origin of each element, statistical correlations between trace elements, major ions, and turbidity have been assessed using the Spearman coefficient (p) (Fig. 7).

The correlation between turbidity and the analyzed components shows notable differences according to the sampling point (surface vs groundwater). Albarrán stream (Fig. 7A) show p values between turbidity and trace elements (Al, P, Mn, and Ni) which range from 0.72 to 0.96 for runoff samples at P1; while at P2, turbidity correlates (0.7–0.79) with P, Mn, and Ba. Major ions show a high correlation (> 0.86) with Li and Sr at P1, but in P2, only Ca^{2+} and HCO_3^- present an apparent correlation (0.66 and 0.62, respectively). Furthermore, the other analyzed elements present a significantly negative correlation with characteristic major ions from carbonate (Mg^{2+}, Ca^{2+}, and HCO_3^-) and evaporite dissolution (Cl^- and SO_4^{2-}). The only observed exception

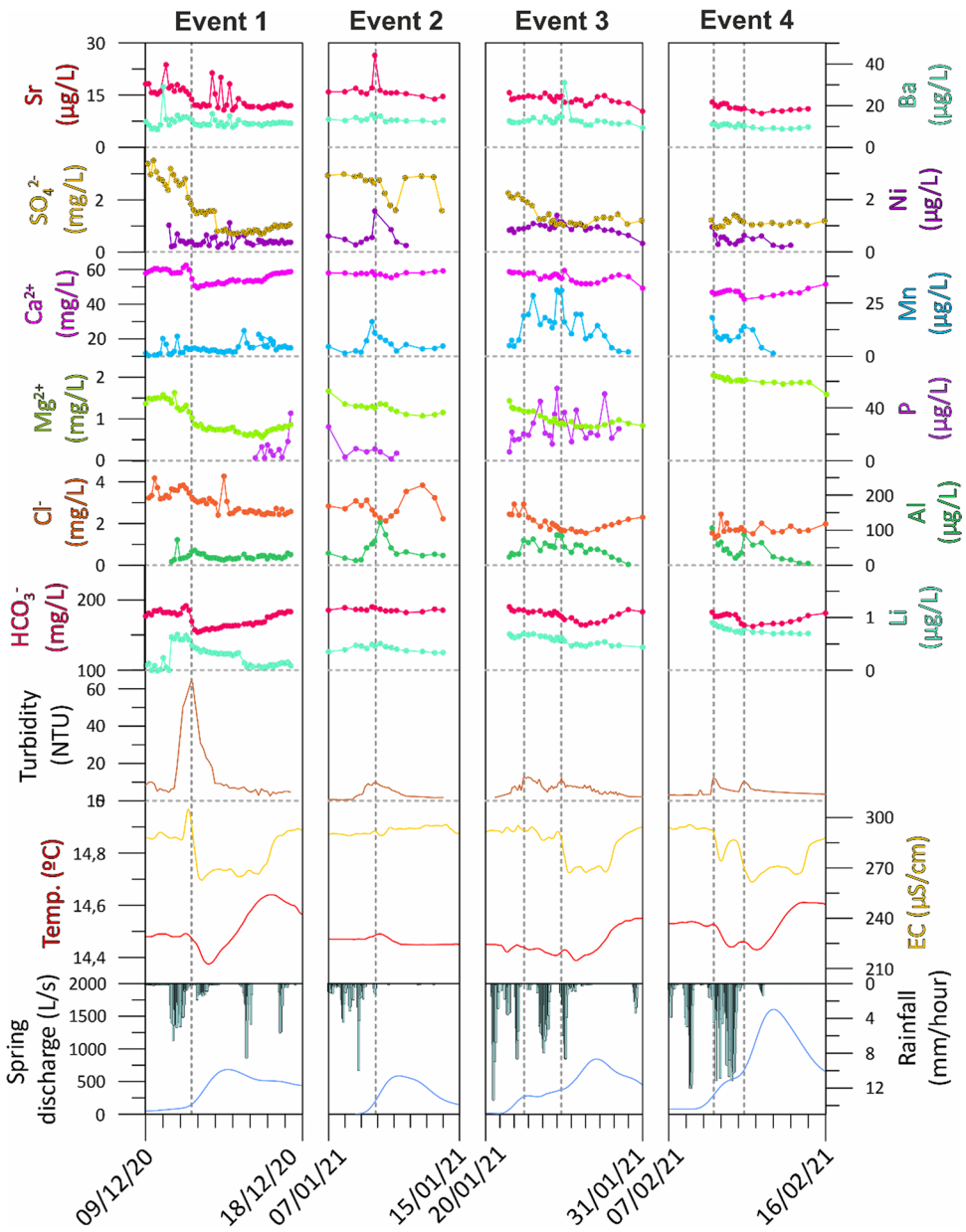

Fig. 5 Time-series of accumulated rainfall, spring discharge, electrical conductivity, temperature, turbidity, major ions, and trace elements in Cornicabra spring water during four selected flood events. Dashed vertical grey line represents turbidity peak/s at each event

is the positive correlation found between P and Ba with Cl^- in P2 (0.85 and 0.52, respectively) and P1 (0.52 and 0.72) (Fig. 7A).

Correlations in groundwater (Fig. 7B) present relatively good correlations ($p > 0.61$) at Cornicabra and Algarrobal springs between turbidity with Al, Mn, and Ni and also between these three elements. It highlights that, in Algarrobal, a quite good correlation of this parameter is also observed with Sr (0.63) and Ba (0.81) in contrast to Cornicabra spring (< 0.43). In comparison to surface water samples, all trace elements present a positive correlation between them. Some individual correlations such as Sr with Ni and Ba (0.73 and 0.81, respectively) in Algarrobal spring and Ni with or Li (0.73), or Ba with Al (0.86) in Cornicabra spring especially highlight (Fig. 7B). The strong correlations found in P1 and P2, such as Sr and Li with major ions or P and Ba with Cl^-, are not observed in groundwater apart from Li with Mg^{2+} (0.7) in Algarrobal spring.

To identify the processes that dominate transport mechanisms on each sampling point, a Principal Component Analysis (PCA) was realized including information from major ions (HCO_3^-, Ca^{2+}, Mg^{2+}, SO_4^{2-}, and Cl^-), trace elements (Li, Al, P, Mn, Ni, Sr, and Ba) and physico-chemical parameters (EC and turbidity) (Fig. 8). The two main components

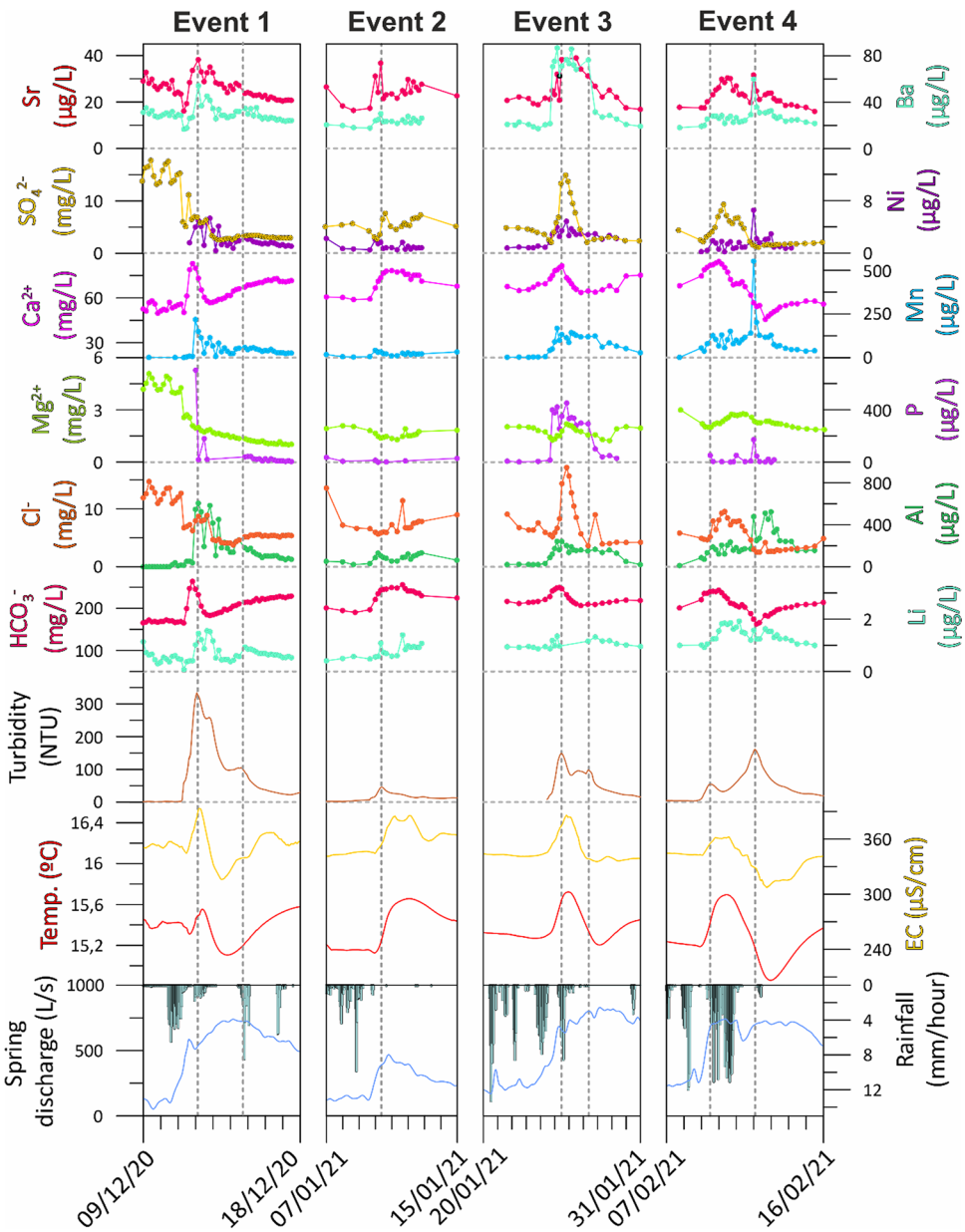

Fig. 6 Time-series of accumulated rainfall, spring discharge, electrical conductivity, temperature, turbidity, major ions, and trace elements in Algarrobal spring water during four selected flood events. Dashed vertical grey represents turbidity peak/s at each event

explain 60.8% of the total variance (Fig. 8A): 44.7% Dimension 1 and 16.1% Dimension 2. The variables are mainly distributed in two big groups, which show a high influence of Dimension 3 (not represented in Fig. 8). Thus, the first group is composed by EC, major ions with Li, P, and Sr, which represent the solute transport. The second group is composed by turbidity together with Al, Mn, Ni, and—to a lesser extent—Ba, which represent sediment transport.

Sample scatter plot (Fig. 8B) displays different dispersion of samples: runoff and WWTP effluent samples show a high dispersion and distribution along Dimension 1, while groundwater samples display a lower dispersion (Algarrobal spring) or—practically—no dispersion (Cornicabra spring).

Hence, considering the two dimensions of the PCA: surface water samples are mainly located towards the positive part of Dimension 1, while the variance in the chemical quality of Algarrobal spring is mainly defined by Dimension 2. The samples from Cornicabra spring are located in the quadrant that includes negative parts of both Dimensions, and are characterized by a lower magnitude of maximum turbidity records during flood episodes and smoother variations of major ions and trace metals.

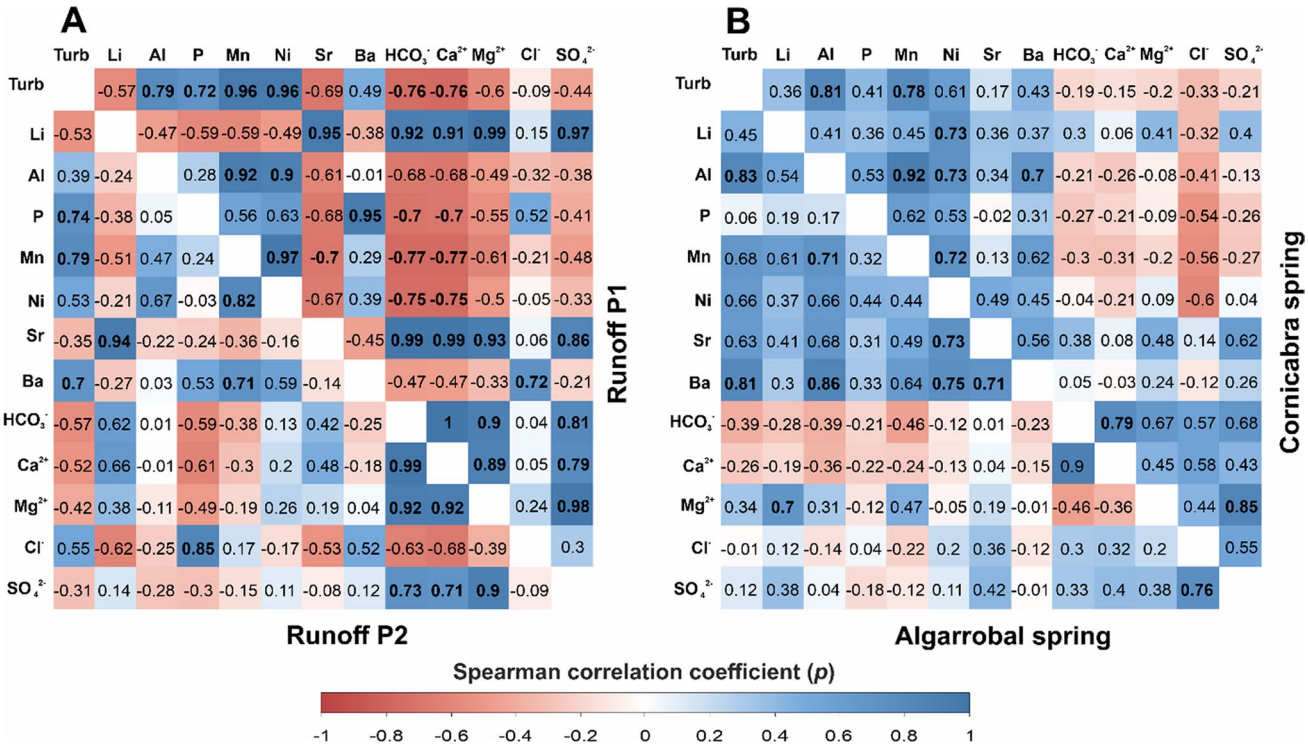

Fig. 7 Spearman coefficient (*p*) correlation matrix among selected trace elements, major ions, and turbidity in runoff waters from Albarrán stream (**A**) and the permanent karst springs (**B**)

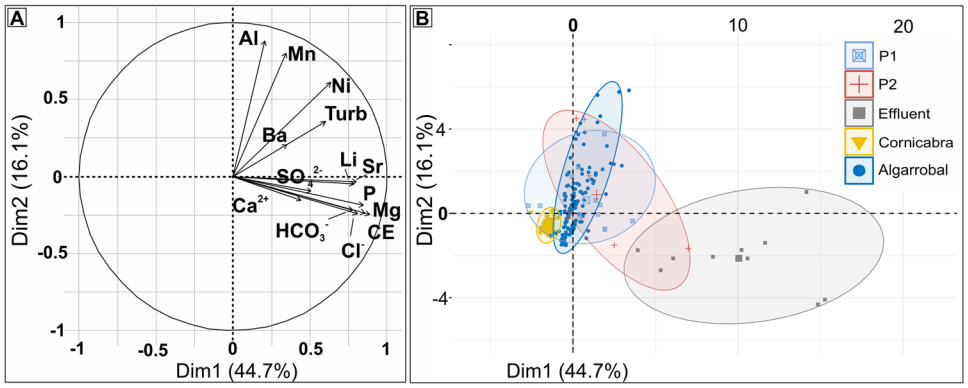

Fig. 8 Principal component analysis done with data from major ions, trace elements, electrical conductivity, and turbidity: **A** hydrochemical variables space; **B** samples scatter plot

Discussion

Occurrence and fate of trace elements

Soil samples

The two types of soils analyzed in this research have different geological origins that determine their mineralogical composition: flysch clays of Albarrán stream (AS) were formed in deep-marine water from turbiditic flows, while *Terra rossa* soils developed over the epikarst (ES) were formed by accumulation of less-soluble minerals during the dissolution (karstification) of carbonate bare rocks. The concentration of trace elements in both AS and ES showed minor differences between them, specifically regarding Li, Mn, and Ni, with higher concentration in ES, and Sr and Ba, enriched in AS (Fig. 3). Mean trace elements concentration in clayey soils (marine clays or *Terra rossa*) found by previous studies (Fig. 9) shows some differences between test sites, but all values for each trace element are within the same order of magnitude. Despite that no remarkable differences were identified between the composition of marine clays (Turekian and Wedepohl 1961; Ruiz Cruz 1999; Lerouge et al. 2017) and *Terra rossa* (Bellanca et al. 1996;

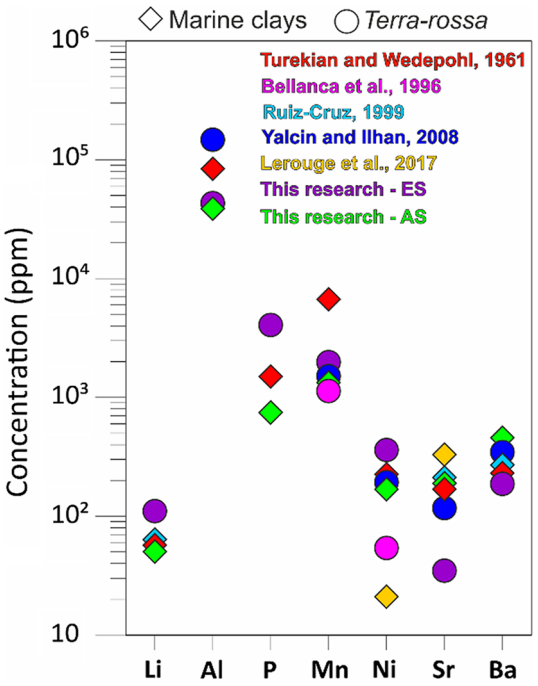

Fig. 9 Trace-element composition of different clayey soils found in previous studies

Yalcin and Ilhan 2008), both types of soils present Al, Mn, and P in higher concentrations than other elements (Fig. 9).

The analyzed trace elements are commonly present in illite, smectite, kaolinite, and chlorite group minerals which might also be present in the soils of the study area. Furthermore, heavy metals, such as Al, Mn, or Ni, may appear as part of the mineralogical background composition of clay minerals (Kumar et al. 2001; Vesper et al. 2001). The geochemistry and composition of *Terra rossa* soils commonly include Al, Mn, with Si and Fe as major elements (Merino and Banerjee 2008) which may then be found as silicates and oxide minerals (Benedetti et al. 1994). Ni is known to occur in pyrite (among other metal sulfides, Campbell and Ethier 1984; Finkelman 1995), which minor presence was described in some clay deposits similar to those in the study area (Ruiz Cruz 1994) and could also explain its presence in AS. However, the existence of reduced species in *Terra rossa* is limited and enhanced Ni content has been traditionally associated with the Mn-rich parts of the ferromanganese nodules (McKenzie 1972; Liu et al. 2002). Given that the presence of evaporite rocks in the Albarrán stream catchment is discarded, the origin of SO_4^{2-} (and related trace elements) might present multiple potential origins, such as the local application of fertilizers or oxidation of metal sulfides from the flysch clays and sandstones (Ruiz Cruz 1994).

Previous studies (Huh et al. 1998; Wang et al. 2015; Charbonnier et al. 2022) demonstrated the implications of silicate weathering in the presence of Li, Ba, and Sr in most stream catchments. However, the proportion of such minerals in the study area should be minor compared to previously mentioned silicates. In addition, carbonate and evaporite rocks might also contain a substantial amount of Sr and Ba in minerals, such as celestite ($SrSO_4$) and barite ($BaSO_4$) (Kilchmann et al. 2004; Goldscheider 2005; Stanienda 2016). Thus, considering that non-anthropogenic contamination exists in the soils' composition represented in Fig. 9, it is possible to assume that the analyzed components in ES and AS are naturally present in such range of concentrations.

Surface water and groundwater samples

The mean concentration of the analyzed trace elements shows clear differences depending on the sampling point, both in surface water and groundwater. The geological formations cropping out in the endorheic areas of Ubrique test site are similar to that of the studies of Ruiz Cruz (1994, 1999) and present clay minerals in which chemical structures, mainly Al, Ni, and Mn—among other trace elements—can be found. Furthermore, these elements display a high correlation ($p > 0.9$) in P1 (Fig. 7) between them, which suggests a common origin in runoff samples without the influence of WWTP leakages. Given that mean Al, Ni, and Mn concentrations in runoff samples collected in Albarrán stream are quite similar in P1 and P2 sampling points and both show higher values compared to mean concentration in WWTP effluent (Table 3), the natural origin of such elements is determined.

Al, Mn, Ni, and turbidity display higher mean values in groundwater samples from Algarrobal spring compared to runoff and Cornicabra water samples (Table 2; Fig. 4). A similar correlation as the one described at P1 is found between these three elements at karst springs, especially evident in the Cornicabra spring (0.7–0.9) with respect to Algarrobal (0.4–0.7, Fig. 7). Karst studies dealing with diffuse recharge systems, with low sediment transfer during flooding events (Jebreen et al. 2018), reported lower Al, Mn, and Ni mean concentrations than in those affected by surface runoff leakages (Ma et al. 2011; Xu et al. 2020). In comparison, Vesper et al. (2001) and Vesper and White (2003) found much higher mean concentration (around one order of magnitude each one compared to this study) of some trace elements, such as Al, Ba, Mn, Ni, and maximum turbidity (up to 589 NTU) in a karst system with a certain influence of concentrated recharge. Such results, together with the enhanced Al and Mn concentrations in Algarrobal spring in comparison to the runoff samples (Table 3), highlight the importance of allochthonous clay sediment contribution as the main source of the more conservative trace elements. Hence, most of the suspended sediments and associated Al, Mn, and Ni detected in water samples are naturally released by runoff weathering of the clayey minerals that compose

the soil of endorheic areas and finally infiltrates into the system.

Li and Sr display higher mean values in runoff samples compared to groundwater (Fig. 4). The good correlation (> 0.9) of such trace elements with the characteristic ions of limestone dissolution (Mg^{2+}, Ca^{2+}, and HCO_3^-) is more evident in the P1 samples rather than P2 or groundwater (Fig. 7). The concentration of these elements in surface water in other karst environments is highly variable and mainly depends on the lithology and land use. For example, in a recent karst river study developed in a rural area from China (Xu et al. 2020), similar concentrations to this study (Table 3) of Li and Sr were measured in surface waters from a catchment in carbonate and siliciclastic rocks. These statements support the hypothesis of a natural origin which might be related to carbonate dissolution form marls outcropping in Albarrán stream catchment.

P and Ba show different correlations and affinities depending on the sampling point but especially correlate at P1 (0.95) and, to a lesser extent, at P2 (0.53, Fig. 4). In addition, both trace elements show an apparent correlation with Cl^- in surface samples, typically related to human activities in absence of evaporite rocks. P and Ba have been commonly associated with anthropic influence from urban sewage systems and industrial emissions. Other hydrogeological studies (Neal et al. 2006; Krishna et al. 2009) dealing with the origin and fate of trace elements in industrialized areas highlighted the potential anthropogenic source of Ba with mean concentrations ranging from 60 to 600 µg/L. The contribution of domestic wastewaters is also known to increase P concentrations (as PO_4^{3-}) over natural inputs (Hardwick 1995; Liao et al. 2020). In this study, mean P concentration is one order of magnitude higher in effluent samples than in runoff waters and a significant increase is observed between P1 and P2 sampling points (Table 3), which suggests a great contribution of P coming from the WWTP. Nonetheless, mean concentration of P in waste waters (Table 3) is included within the normal range measured in municipal wastewaters (4–16 mg/L) (Metcalf and Eddy Inc. 2003).

In groundwater samples, mean concentrations of Li, Sr, and Ba (Table 3) are comparable to those found in other non-polluted karst systems, with characteristic values from carbonate rock weathering (mean concentrations between 1 and 2 µg/L of Li, 150 and 200 µg/L of Sr, and 11 and 40 µg/L of Ba; Kilchmann et al. 2004; Jebreen et al. 2018). However, the rise of Sr and Ba concentrations in Algarrobal spring together with turbidity increases (Fig. 6) is much evident than in Cornicabra (Fig. 5) and suggests a higher influence of allogenic recharge. In this research, the higher mean concentration and variability of such elements in Albarrán catchment soil (AS, Fig. 3) and runoff waters (Fig. 4), rather than ES and groundwater, may indicate that the availability of such elements is enhanced in silicate-clayey lithologies or dilution processes occur within the system (or combination of both).

The time-series of elemental P in karst groundwater did not show a clear pattern in the successive events (Figs. 5, 6) but its presence is significantly higher and more defined in Algarrobal spring (Table 3), which shows maximum appreciable peaks in Fig. 6. Despite that P is naturally present in diverse ecosystems and karst environments (Imbach 1993; Markovic et al. 2019) as PO_4^{3-} with concentrations that may range between 50 and 900 µg/L for karstic springs, such ion was not detected through ion chromatography in this research. P might then be considered as a minor component in the karst springs due to its low concentration, but a major element in runoff (P1 and P2) samples in the WWTP effluent. Hence, the origin of P is probably related to human activities in Ubrique system.

Factors conditioning mobility of trace elements

The statistical analysis developed in "Statistical relationships between trace elements and transport vector" section revealed two major trends among trace elements and transport carriers (turbidity vs major ions). Some elements (Al, Mn, Ni, and Ba) presented in surface and groundwater a good correlation with turbidity and its chemical variability explained, to a major extent, by this physical parameter. The rest of the elements analyzed (Li, Sr, and P) present a higher affinity with the major ions and PCA grouping with electrical conductivity.

Transport related to suspended sediments

The statistical analysis (PCA) carried out in this study shows an association between Al, Mn, and Ni with turbidity (Fig. 8), and a Spearman correlation coefficient of $p > 0.68$ (Fig. 7) in both surface and groundwater. Different physicochemical variables might influence sediment transport in groundwater, as the number of large particles and colloids appears to be determined by discharge, pH, and temperature (Atteia and Kozel 1997; Herman et al. 2012). However, in this research, the increases in the hydraulic head of the system at the beginning of each flood are responsible for the greatest turbidity variability.

Acid rain might favour chemical weathering processes such as hydrolysis that dissolves ions from the clay mineral and enhances trace elements (Al, Mn and Ni) mobility (Sposito 1996). Speciation of these trace elements in water is characterized by the combination of hydroxyl groups with Al, Mn^{2+} and Ni^{2+} (Stumm and Morgan 1981; Hem 1985; Perkins and Mason 2015). The subsequent pH and temperature conditions or surface chemical bond group will condition the occurrence of surface complexation or electrostatic attraction processes of metals onto solids. These

processes constitute common phenomena in natural systems (Hart 1982; Jenne and Zachara 1987; Horowitz 1991; Cholet et al. 2019) and its enhanced mobility by sediment transport through karst aquifers may account for high concentrations at the springs. As well as previously suggested by Vesper and White (2003), Al is proposed in this research as a sediment proxy given its analogue transport with suspended sediments and other trace elements, such as Mn and Ni, because of its high correlation ($R^2 > 0.94$) with turbidity.

Moreover, Ba also shows a high correlation with turbidity in surface sampling points and Algarrobal spring (Fig. 7). Despite that this element presents an anthropogenic origin, sorption processes onto solids have also been widely described (Eylem et al. 1990; Atun and Bascetin 2004). This would also explain the enhanced Ba concentration in Algarrobal spring due to the high turbidity records. Thus, the direct implication of suspended sediments (represented as turbidity) on Al, Mn, Ni, and Ba transport is clearly observed in surface and groundwater samples in Ubrique test site.

Transport related to dissolved ions

Despite that the processes that control Sr, P, and Li transport in runoff and groundwater must be the same, slight differences are observed. An apparent correlation between Li and Sr and most representative major ions (HCO_3^- and SO_4^{2-}) is found (Figs. 5, 6) and emphasized in runoff samples (Fig. 7). Such elements might be present in aqueous solution as hydrated mono- or di-valent cations, without the need for aqueous complexation (Hanor 2000).

The dominant factors controlling the mobility of Li and Sr in surface appears to be solute transport mainly associated with HCO_3^-. A similar process is observed with P, which, despite of its complex chemical behavior, the mobility of this trace element appears to be dominated by solute migration (Fig. 8). The concentration of these elements is much lower in groundwater compared to surface water (Fig. 4), which indicates that dilution processes might occur due to the arrival of recently infiltrated rainwater through diffuse recharge and posterior mixing with waters from the saturated zone.

Both springs show an abrupt depletion in the concentration of SO_4^{2-} of the first event in comparison to the following ones. In addition, a decreasing trend is also observed in the concentration of some elements such as Sr and Cl^- throughout the four events analyzed (Figs. 5, 6). This circumstance can be directly related to the saturated zone thickness prior to the event and the recharge conditions. Hence, spring response defining Event 1 is especially particular due to the absence of rainfall in the previous 6 months, resulting in a greater residence time of the groundwater drained at the beginning of the event in both springs and, therefore, a greater concentration of dissolved ions such as SO_4^{2-}, Cl^- or Mg^{2+}.

Assessment of relative contribution of allogenic recharge to spring flow

The different minerals and available elements found in catchment soils (Fig. 3) as well as the chemical signature of aquifer rocks might be expressed as specific ratios in water samples. Previous studies (Land et al. 1998, 2000) used specific molar ratios, as Ca/Sr, as effective tracers for analyzing aquifer–river interactions assuming differential concentrations of mineral phases. The authors successfully identified the influence of surface recharge flows in a shallow porous aquifer with mainly silicate and clay minerals using Ca/Sr jointly to Ba/Sr molar ratio. Hogan and Blum (2003) coupled this technique with water isotopes in a small (1.2 km^2) carbonate–silicate river catchment and found a decrease of Ca/Sr ratio during storm events.

In this research, this approach, coupled to Ba content, is used to assess the relative contribution of allogenic recharge in terms of groundwater chemical variability. To validate the application of this method, Al concentration (interpreted as sediment proxy) is represented as symbol size. Hence, Fig. 10 shows, on the one hand, the content in Ba is notably higher (> 0.3 meq/L) in surface water samples (followed by WWTP Effluent, Table 3) rather than in groundwater samples. On the other hand, Ca/Sr ratio shows a characteristic value (between 20 and 23) in groundwater samples collected during low water conditions, while runoff samples present specific molar ratio values of Ca/Sr < 7.

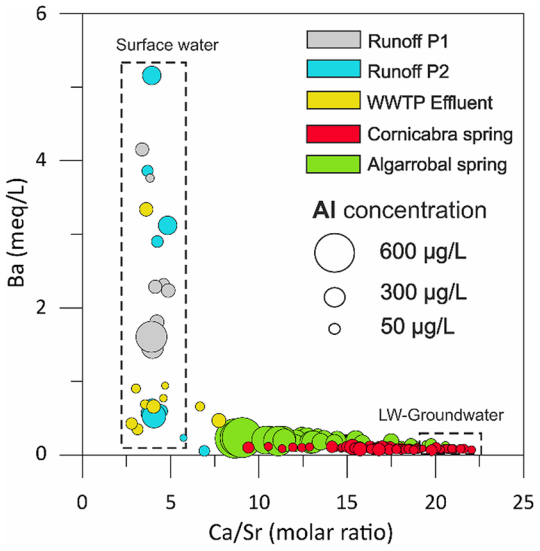

Fig. 10 Relationship between Ba (meq/L) and Ca/Sr molar ratio in runoff and groundwater samples. Al concentration (µg/L) is represented as a function of symbol size

Groundwater samples obtained during flooding events are distributed within the Ca/Sr molar ratio range between 7 and 20 show a slightly increasing trend of Ba. Moreover, Al content apparently increases towards lower Ca/Sr ratios, which is especially notable in Algarrobal spring. Given the high correlation between Al and turbidity, it is possible to assume that allogenic recharge constitutes the main contribution of suspended sediment into the karst system. However, this spring presents much higher turbidity and Al content compared to runoff samples (Fig. 10; Table 2) which indicate that sediment storage might exist inside the system conduits and is posteriorly mobilized to the spring. This process is evidenced in the extremely high turbidity record in Event 1, which shows the most abrupt response in both springs, as reflected by hydrochemistry. The low hydrodynamic stage of the system in the first event of the hydrological year might then be determinant in the accumulation and deposition of sediments within the conduits network.

As a general trend, groundwater samples form Algarrobal spring show a higher similarity with runoff Ca/Sr molar ratios (Fig. 10) as well as higher content in the analyzed trace elements compared to Cornicabra spring. These results suggest a notably higher influence of allogenic recharge in terms of sediment input and chemical variability derived from allogenic recharge in Algarrobal spring. Despite that, in this preliminary research, it is not possible to estimate a quantitative contribution, these results are coherent with the results derived from the dye experiment previously realized in this test site (Martín-Rodríguez et al. 2023). These findings have direct implications in drinking water capture at the springs, given that the leakages from the WWTP are potentially connected to the main outlets.

Conclusions

The developed multi-criteria approach combining physical (spring discharge, turbidity, temperature, and electrical conductivity) and chemical (major ions and trace elements) data has been successfully tested to investigate recharge dynamics and vulnerability to contamination in a binary karst aquifer. The proposed framework is based on two main elements: a complete monitoring network (including climate, soil, and natural waters from permanent springs used for water supply and wastewater) and a high-periodicity water sampling strategy.

In this research, the analyzed trace elements in soil samples were measured within the normal range of clayey soils in the absence of anthropogenic influence and chemical anomalies. Chemical weathering of clayey and carbonate materials found in the main allogenic recharge catchment is responsible for the presence of Al, Mn, Ni, Li, and Sr, in water samples. In contrast, the source of Ba and P was determined to present a major anthropogenic contribution. The transport of sediment and some trace elements (Al and Mn and to a minor extent, Ni and Ba) is intrinsically related due to the chemical nature of colloids. Hence, Al has been proposed in this test site as the optimal sediment proxy given its high correlation with turbidity in groundwater samples.

The analysis of long-term time-series is essential in karst aquifers to provide a better comprehension of the data variability. In this study, the hydrodynamic conditions of the aquifer prior to individual rain events and their magnitude proved to present direct implications in trace elements transport and sediment storage and mobilization. Hence, vulnerability is enhanced after long dry periods due to the accumulation of sediments and related trace elements within the karst system. The analysis of karst spring response through time-series and the determination of specific Ca/Sr molar ratios together with Ba content revealed a higher relative contribution of allogenic recharge to Algarrobal spring compared to Cornicabra in terms of sediment transport and hydrochemical variability.

The findings achieved in this study evidence the potential benefits of combining high-periodicity monitoring and complementary laboratory analysis for a correct vulnerability assessment in water systems with a high temporal variability of chemical parameters. The methodological framework applied in this research provides a comprehensive knowledge of recharge mechanisms of the binary karst system, which is highly important for a proper management of groundwater resources. This site-specific approach is easily transferrable to different karst water systems captured for human consumption.

Acknowledgements The authors would like to thank the local government of Ubrique town, the local water company "Empresa Mixta de Aguas de Ubrique" and the authorities of the Sierra de Grazalema Natural Park for its collaborative behavior.

Author contributions All authors contributed to the study conception and design. Data collection and analysis, material preparation, and manuscript writing were performed by JFO. Revision and discussion on the first and successive versions of the manuscript was realized by JAB and BA. All authors have carefully read the article and approved the final version of the manuscript.

Funding Funding for open access publishing: Universidad Málaga/CBUA This research is a contribution to the PRIMA funded European project KARMA (Karst Aquifer Resources availability and quality in the Mediterranean Area—ANR-18-PRIM-0005), the Spanish project, PCI2019-103675 of the Joint International Actions Programme of the Ministry of Science, Innovation and Universities as well as by the project PID2019-111759RB-I00 and the Research Group RNM-308 of the Junta de Andalucía, funded by the Autonomous Government of Andalusia (Spain). Funding for open access charge: Universidad de Málaga / CBUA.

Data availability All the data related to the manuscript are reported within the paper and available from the corresponding author upon request.

Declarations

Competing interests The authors declare that they have no competing financial interests or personal relationships that could have appeared to influence the work reported in this paper.

References

Adriano DC (1986) Heavy metals in the environment. Springer-Verlag, New York

Atteia O, Kozel R (1997) Particle size distributions in water from a karstic aquifer: from particles to colloids. J Hydrol 201:102–119

Atun JG, Bascetin E (2004) Adsorption of barium on kaolinite, illite and montmorillonite at various ionic strengths. Radiochim Acta 91:223–228

Bellanca A, Hauser S, Neri R, Palumbo B (1996) Mineralogy and geochemistry of *Terra rossa* soils, western Sicily: insights into heavy metal fractionation and mobility. Sci Total Environ 193(1):57–67. https://doi.org/10.1016/S0048-9697(96)05336-3

Benedetti MF, Menard O, Noack Y, Carvalho A, Nahon D (1994) Water–rock interactions in tropical catchments: field rates of weathering and biomass impact. Chem Geol 118:203–220. https://doi.org/10.1016/0009-2541(94)90177-5

Buss HL, Lara MC, Moore OW, Kurtz AC, Schulz MS, White AF (2017) Lithological influences on contemporary and long-term regolith weathering at the Luquillo Critical Zone Observatory. Geochim Cosmochim Acta 196:224–251. https://doi.org/10.1016/j.gca.2016.09.038

Campbell FA, Ethier VG (1984) Nickel and cobalt in pyrrhotite and pyrite from the Faro and Sullivan orebodies. Can Mineral 22:503–506

Charbonnier Q, Bouchez J, Gaillardet J, Calmels D, Dellinger M (2022) The influence of black shale weathering on riverine barium isotopes. Chem Geol 594:120741. https://doi.org/10.1016/j.chemgeo.2022.120741

Cholet C, Steinmann M, Charlier JB, Denimal S (2019) Characterizing fluxes of trace metals related to dissolved and suspended matter during a storm event: application to a karst aquifer using trace metals and rare earth elements as provenance indicators. Hydrogeol J 27:305–319. https://doi.org/10.1007/s10040-018-1859-2

Currens JC (1997) A sampling plan for conduit-flow karst springs: Minimizing sampling cost and maximizing statistical utility. In: Sixth multidisciplinary conference on sinkholes and the engineering and environmental impacts of karst, Springfield, Missouri, pp 193–198. https://doi.org/10.1016/S0013-7952(98)00064-7

Cutillas-Barreiro L, Pérez-Rodríguez P, Gómez-Armesto A, Arias-Estévez M, Novoa-Munoz JC, Fernández-Sanjurjo MJ, Álvarez-Rodríguez E, Núnez-Delgado A (2016) Lithological and land-use based assessment of heavy metal pollution in soils surrounding a cement plant in SW Europe. Sci Total Environ 562:179–190. https://doi.org/10.1016/j.scitotenv.2016.03.198

De Kimpe CR, Laverdiere MR, Dejou J, Lasalle P (1984) Effects of acidic and basic parent materials on formation of some soils in Quebec (Canada). Geoderma 33(2):101–118. https://doi.org/10.1016/0016-7061(84)90023-5

Dragović R, Gajić B, Dragović S, Đorđević M, Đorđević M, Mihailović N, Onjia A (2014) Assessment of the impact of geographical factors on the spatial distribution of heavy metals in soils around the steel production facility in Smederevo (Serbia). J Clean Prod 84:550–562. https://doi.org/10.1016/j.jclepro.2014.03.060

Durn G, Perkovic I, Stummeyer J, Ottner F, Mileusnic M (2021) Differences in the behaviour of trace and rare-earth elements in oxidizing and reducing soil environments: case study of *Terra rossa* soils and cretaceous palaeosols from the Istrian peninsula, Croatia. Chemosphere 283:131286. https://doi.org/10.1016/j.chemosphere.2021.131286

Elderfield H, Bertram CJ, Erez J (1996) A biomineralization model for the incorporation of trace elements into foraminiferal calcium carbonate. Earth Planet Sci Lett 142:409–423. https://doi.org/10.1016/0012-821X(96)00105-7

Eylem C, Erten HN, Goktürk H (1990) Sorption-desorption behaviour of barium on clays. J Environ Radioact 11(2):183–200

Feeser I, O'Connell M (2009) Fresh insights into long-term changes in flora, vegetation, land use and soil erosion in the karstic environment of the Burren, western Ireland. J Ecol 97(5):1083–1100

Finkelman RB (1995) Modes of occurrence of environmentally-sensitive trace elements in coal. In: Swaine DJ, Goodarzi F (eds) Environmental aspects of trace elements in coal. Energy and environment, vol 2. Springer, Dordrecht

Gill LW, Babechuk MG, Kamber BS, McCormack T, Murphy C (2018) Use of trace and rare earth elements to quantify autogenic and allogenic inputs within a lowland karst network. Appl Geochem 90:101–114. https://doi.org/10.1016/j.apgeochem.2018.01.001

Goldscheider N (2005) Karst groundwater vulnerability mapping: application of a new method in the Swabian Alb, Germany. Hydrogeol J 13(4):555–564. https://doi.org/10.1007/s10040-003-0291-3

Goldscheider N, Drew D (2007) Methods in karst hydrogeology. IAH international contributions to hydrogeology, vol 26. CRC, Boca Raton, FL

Grolimund D, Barmettler K, Borkovec M (2007) Colloid facilitated transport in natural porous media: fundamental phenomena and modelling. In: Frimmel FH, von der Kammer F, Flemming H-C (eds) Colloidal transport in porous media. Springer, Berlin, Heidelberg, pp 3–27

Hanor JS (2000) Barite–celestine geochemistry and environments of formation. In: Alpers CN, Jambor JL, Nordstrom DK (eds) Sulfate minerals: crystallography, geochemistry, and environmental significance. Reviews in mineralogy and geo-chemistry, vol 40. Mineralogical Society of America and the Geochemical Society, Washington, DC, pp 193–263

Hardwick P (1995) The impact of agriculture on limestone caves with special references to the Castleton Catchment. Unpubl. PhD thesis, Manchester Metropolitan University

Hart BT (1982) Uptake of trace metals by sediments and suspended particulates: a review. Hydrobiologia 91:299–313. https://doi.org/10.1007/BF00940121

Hem JD (1985) Study and interpretation of the chemical characteristics of natural water, 3rd edn. US Geological Survey Water-Supply Paper 2254

Herman EK, Toran L, White WB (2012) Clastic sediment transport and storage in fluviokarst aquifers: an essential component of karst

hydrogeology. Carbonates Evaporites 27:211–241. https://doi.org/10.1007/s13146-012-0112-7
Hogan JF, Blum JD (2003) Tracing hydrologic flow paths in a small forested watershed using variations in 87Sr//86Sr, [Ca]/[Sr], [Ba]/[Sr] and $\delta^{18}O$. Water Resour Res. https://doi.org/10.1029/2002WR001856
Horowitz AJ (1991) A primer on sediment-trace element chemistry, 2nd edn. Lewis Publishers Inc, Michigan, p 136
Huh Y, Chan LH, Zhang L, Edmond JM (1998) Lithium and its isotopes in major world rivers: implications for weathering and the oceanic budget. Geochim Cosmochim Acta 12:2039–2051. https://doi.org/10.1016/S0016-7037(98)00126-4
Imbach T (1993) Environmental hydrogeology of a karst system with thermal and normal groundwaters: examples from the Bursa region (Turkey). In: Proc hydrogeological processes in Karst Terranes, IAHS Publ. No. 207, pp 7–13
Jebreen H, Banning A, Wohnlich S, Niedermayr A, Ghanem M, Wisotzky F (2018) The influence of karst aquifer mineralogy and geochemistry on groundwater characteristics: West Bank, Palestine. Water 10(12):1829. https://doi.org/10.3390/w10121829
Jenne EA, Zachara JM (1987) Factors influencing the sorption of metals. In: Dickson KL, Maki AW, Brungs WA (eds) Fate and effects of sediment-bound chemicals. Pergamon Press, New York, pp 83–98
Kilchmann S, Waber HN, Parriaux A, Bensimon M (2004) Natural tracers in recent groundwaters form different alpine aquifers. Hydrogeol J 12:643–661
Kong XT (2014) China must protect high-quality arable land. Nature 506(7486):7. https://doi.org/10.1038/506007a
Krishna AK, Satyanarayanan M, Govil PK (2009) Assessment of heavy metal pollution in water using multivariate statistical techniques in an industrial area: a case study from Patancheru, Medak District, Andhra Pradesh, India. J Hazard Mater 167(1):366–373. https://doi.org/10.1016/j.jhamat.2008.12.131
Kumar AV, Patil RS, Nambi KSV (2001) Source apportionment of suspended particulate matter at two traffic junctions in Mumbai, India. Atmos Environ 35(25):4245–4251. https://doi.org/10.1016/S1352-2310(01)00258-8
Land M, Ingri J, Andersson PS, Ohlander BC (1998) Tracing subsurface water flow paths by means of dissolved Ba/Sr, Ca/Sr and 87Sr/86Sr ratios. Min Mon 62(2):850–851
Land M, Ingri J, Andersson P, Ohlander BC (2000) Ba/Sr, Ca/Sr and Sr-87/Sr-86 ratios in soil water and groundwater: implications for relative contributions to stream water discharge. Appl Geochem 15:311–325. https://doi.org/10.1016/S0883-2927(99)00054-2
Lerouge C, David K, Claret F, Debure M, Grangeon S, Madé B, Montavon G, Tournassat C (2017) Role of carbonate minerals in the distribution of trace elements in marine clay formations. Proc Earth Planet Sci 17:798–801. https://doi.org/10.1016/j.proeps.2017.01.043
Li X, Xie Y, Wang J, Christakos G, Si J, Zhao H, Ding Y, Li J (2013) Influence of planting patterns on fluoroquinolone residues in the soil of an intensive vegetable cultivation area in northern China. Sci Total Environ 458:63–69. https://doi.org/10.1016/j.scitotenv.2013.04.002
Liao R, Hu J, Li Y, Li S (2020) Phosphorus transport in riverbed sediments and related adsorption and desorption characteristics in the Beiyun River, China. Environ Pollut 266:115153. https://doi.org/10.1016/j.envpol.2020.115153
Liu F, Colombo C, Adamo P, He JZ, Violante A (2002) Trace elements in manganese–iron nodules from a Chinese Alfisol. Soil Sci Soc Am J 66:661–670. https://doi.org/10.2136/sssaj2002.6610
Ma R, Wang Y, Sun Z, Zheng C, Ma T, Prommer H (2011) Geochemical evolution of groundwater in carbonate aquifers in Taiyuan, northern China. Appl Geochem 26(5):884–897. https://doi.org/10.1016/j.apgeochem.2011.02.008
Mahler BJ, Lynch FL (1999) Muddy waters: temporal variation in sediment discharging from a karst spring. J Hydrol 214:165–178. https://doi.org/10.1016/S0022-1694(98)00287-X
Mahler BJ, Lynch L, Bennett PC (1999) Mobile sediment in an urbanizing karst aquifer: implications for contaminant transport. Environ Geol 39(1):25–38. https://doi.org/10.1007/s002540050434
Markovic S, Liang AQ, Watson SB, Guo J, Mugalingam S, Arhonditsis G, Morley A, Dittrich M (2019) Biogeochemical mechanisms controlling phosphorus diagenesis and internal loading in a remediated hard water eutrophic embayment. Chem Geol 514:122–137. https://doi.org/10.1016/j.chemgeo.2019.03.031
Martín-Algarra M (1987) Evolución geológica alpina del contacto entre las Zonas Internas y Externas de la Cordillera Bética. Disseration, University of Granada, Spain, 1171 pp
Martín-Rodríguez JF, Mudarra M, De la Torre B, Andreo B (2023) Towards a better understanding of time-lags in karst aquifers by combining hydrological analysis tools and dye tracer tests. Application to a binary karst aquifer in southern Spain. J Hydrol 621:129643. https://doi.org/10.1016/j.jhydrol.2023.129643
Mavrocordatos D, Mondi-Couture C, Atteia O, Leppard GG, Perret D (2000) Formation of a distinct class of Fe–Ca(–C-org)-rich particles in a complex peat-karst system. J Hydrol 237(3–4):234–247. https://doi.org/10.1016/S0022-1694(00)00309-7
McCarthy JF, McKay LD (2004) Colloid transport in the subsurface: past, present, and future challenges. Vadose Zone J 3(2):326–337. https://doi.org/10.2136/vzj2004.0326
McCarthy JF, Shevenell L (1998) Processes controlling colloid composition in a fractured and karstic aquifer in eastern Tennessee USA. J Hydrol 206(3–4):191–218. https://doi.org/10.1016/S0022-1694(98)00107-3
McKenzie RM (1972) The sorption of some heavy metals by the lower oxides of manganese. Geoderma 8:29–35. https://doi.org/10.1016/0016-7061(72)90030-4
Merino E, Banerjee A (2008) *Terra rossa* genesis, implications for karst, and eolian dust: a geodynamic thread. J Geol 116:62–75. https://doi.org/10.1086/524675
Metcalf and Eddy Inc (2003) Wastewater engineering: treatment and reuse, 4th edn. McGraw-Hill, New York
Neal C, Neal M, Hill L, Wickham H (2006) The water quality of the River Thame in the Thames Basin of south/south-eastern England. Sci Total Environ 360(1–3):254–271. https://doi.org/10.1016/j.scitotenv.2005.08.039
Perkins RB, Mason CE (2015) The relative mobility of trace elements from short-term weathering of a black shale. Appl Geochem 56:67–79. https://doi.org/10.1016/j.apgeochem.2015.01.014
Pronk M, Goldscheider N, Zopfi J (2007) Particle-size distribution as indicator for faecal bacteria contamination of drinking water from karst springs. Environ Sci Technol 41(24):8400–8405. https://doi.org/10.1021/es071976f
Ruiz Cruz M (1994) Diagenetic development of clay and related minerals in deep water sandstones (S. Spain): evidence of lithological control. Clay Miner 29(1):93–104. https://doi.org/10.1180/claymin.1994.029.1.11
Ruiz Cruz M (1999) Clay mineral assemblages in flysch from the Campo de Gibraltar area (Spain). Clay Miner 34(2):345–364. https://doi.org/10.1180/000985599546145
Ryan M, Meiman J (1996) An examination of short-term variations in water quality in a karst spring in Kentucky. Ground Water 34(1):23–30. https://doi.org/10.1111/j.1745-6584.1996.tb01861.x
Sánchez D, Barberá JA, Mudarra M, Andreo B, Martín JF (2018) Hydrochemical and isotopic characterization of carbonate aquifers under natural flow conditions, Sierra Grazalema Natural Park, Southern Spain. Geol Soc London Spec Publ 466:275–293. https://doi.org/10.1144/SP466.16

Sandén P, Karlsson S, Duker A, Ledin A, Lundman L (1997) Variations in hydrochemistry, trace metal concentration and transport during a rain storm event in a small catchment. J Geochem Explor 58:145–155. https://doi.org/10.1016/S0375-6742(96)00078-7

Shevenell L, McCarthy JF (2002) Effects of precipitation events on colloids in a karst aquifer. J Hydrol 255:50–68. https://doi.org/10.1016/S0022-1694(01)00510-8

Sposito G (1996) The environmental chemistry of Aluminium. CRC Press, Florida

Stallard R (2012) Weathering, landscape equilibrium, and carbon in four watersheds in Eastern Puerto Rico. In: Murphy SF, Stallard RF (eds) Water quality and landscape processes of four watersheds in eastern Puerto Rico. Geological Survey Professional Paper, US Geological Survey, Reston, Virginia, pp 199–262

Stanienda K (2016) Strontium and barium in the triassic limestone of the opole Silesia deposits. Arch Min Sci 61(1):29–46. https://doi.org/10.1515/amsc-2016-0003

Stevanović Z (2019) Karst waters in potable water supply: a global scale overview. Environ Earth Sci 78:662. https://doi.org/10.1007/s12665-019-8670-9

Stumm W, Morgan JJ (1981) Aquatic chemistry, 2nd edn. John Wiley, Brisbane, p 780

Turekian KK, Wedepohl KH (1961) Distribution of the elements in some major units of the Earth's crust. Geol Soc Am Bull 72:175–192. https://doi.org/10.1130/0016-7606(1961)72[175:DOTEIS]2.0.CO;2

Turner A (2019) Trace elements in laundry dryer lint: a proxy for household contamination and discharges to waste water. Sci Total Environ 665:568–573. https://doi.org/10.1016/j.scitotenv.2019.02.025

U.S. EPA (U.S. Environmental Protection Agency) (1996) Method 3050B: acid digestion of sludges, sediments, and soils, revision 2. Washington DC. https://www.epa.gov/sites/production/files/2015-06/documents/epa-3050b.pdf

U.S. EPA (U.S. Environmental Protection Agency) (2018) Integrated risk information system (IRIS). United States Environmental Protection Agency. http://www.epa.gov/iris/

Vesper DJ, White WB (2003) Metal transport to karst springs during storm flow: an example from Fort Campbell, Kentucky/Tennessee, USA. J Hydrol 276(1–4):20–36. https://doi.org/10.1016/S0022-1694(03)00023-4

Vesper D, Loop C, White W (2001) Contaminant transport in karst aquifers. Theor Appl Karstol 13:101–111

Wang QL, Chetelat B, Zhao ZQ, Ding H, Li SL, Wang BL, Li J, Liu XL (2015) Behavior of lithium isotopes in the Changjiang River system: sources effects and response to weathering and erosion. Geochim Cosmochim Acta 151:117–132. https://doi.org/10.1016/j.gca.2014.12.015

Xu S, Lang Y, Zhong J, Xiao M, Ding H (2020) Coupled controls of climate, lithology and land use on dissolved trace elements in a karst river system. J Hydrol 591:125328. https://doi.org/10.1016/j.jhydrol.2020.125328

Yalcin MG, Ilhan S (2008) Major and trace element geochemistry of *Terra rossa* soil in the Kucukkoras region, Karaman, Turkey. Geochem Int 46(10):1038–1054. https://doi.org/10.1134/S0016702908100 08X

Yang ZS, Yang LF, Zhang BS (2010) Soil erosion and its basic characteristics at karst rocky-desertified land consolidation area: a case study at Muzhe Village of Xichou County in Southeast Yunnan, China. J Mt Sci 7(1):55–72

Zimmerman LA (1993) Trace metal-suspended particulate matter associations in a fluvial system: physical and chemical influences. In: Rao SS (ed) Particulate matter and aquatic contaminants. Lewis Publishers, Boca Raton, pp 127–155